Improved Sensitivity and Mass Range in Time-of-Flight Bioaerosol Mass Spectrometry Using an Electrostatic Ion Guide

Gregg A. Czerwieniec, Scott C. Russell, and Carlito B. Lebrilla
Department of Chemistry, University of California, Davis, California, USA

Keith R. Coffee, Vincent Riot, Paul T. Steele, Matthias Frank, and Eric E. Gard
Lawrence Livermore National Laboratory, Livermore, California, USA

Bioearosol mass spectrometry (BAMS) analyzes single particles in real time from ambient air, placing strict demands on instrument sensitivity. Modeling of the BAMS reflectron time of flight (TOF) with SIMION revealed design limitations associated with ion transmission and instrument sensitivity at higher masses. Design and implementation of a BAMS linear TOF with electrostatic ion guide and delayed extraction capabilities has greatly increased the sensitivity and mass range relative to the reflectron design. Initial experimental assessment of the new instrument design revealed improved sensitivity at high masses as illustrated when using standard particles of cytochrome C ($m/z \sim 12{,}000$), from which the compound's monomer, dimer ($m/z \sim 24{,}000$) and trimer ($m/z \sim 36{,}000$) were readily detected. (J Am Soc Mass Spectrom 2005, 16, 1866–1875) © 2005 American Society for Mass Spectrometry

Bioaerosol mass spectrometry (BAMS) has recently shown the ability to distinguish single *Bacillus* spores from *Bacillus* vegetative cells [1]. BAMS analyzes single cells without sample pretreatment or preconcentration [2]. Mass spectrometry uses the detection of distinct cellular components (biomarkers) to characterize bacteria and viruses. The small sample size makes strong demands on the instrument in terms of sensitivity. The BAMS reflectron mass spectra of *Bacillus* spores and vegetative cells were limited to signals under m/z 300 [2]. Improving the high mass sensitivity will widen the fingerprint space, allowing for detection of more robust species-specific biomarkers. The reason for the limited mass range is believed to be twofold: failure to readily ionize large biomolecules and poor instrument sensitivity for large ions.

Sampling standard particles composed of mixtures of matrix-assisted laser desorption ionization (MALDI) matrix and analyte provides a means to produce ions of a given m/z [3–5] and assess the instrument performance over a range of masses. The reflectron time-of-flight (TOF) instrument was unable to detect ion signals from standard MALDI particles of angiotensin (MW = 1297 Da) and α-cyclodextrin (MW = 973 Da) but readily detected matrix ions. MALDI particles containing high amounts of gramicidin S (MW = 1140 Da) produced a very weak molecular ion signal. These observations reveal a bias of the reflectron instrument toward lower masses. The removal of this limitation is the subject of the current study. Improving the overall instrument sensitivity for improved biomarker detection from microorganisms may also require additional developments to efficiently generate larger ions from the cells.

Experimental

Particle Generation and Sampling

Aerosol particles were generated from solution via a Collison nebulizer (TSI, Inc., Shoreview, MN). Single particle MALDI experiments provide a suitable system to access the performance of the instrument [5–7]. Gramicidin S particles were generated from a 50/50 H_2O/ethanol solution of 2,5-dihydroxybenzoic acid (DHB; 3×10^{-3}M) and gramicidin S at a 100:1 matrix-to-analyte molar ratio. Cytochrome *c* particles were generated via a saturated solution of sinapinic acid and 0.1% TFA (trifluoroacetic acid). Nebulized particles were passed through a silica-drying column and sampled into the instrument at a 1-L/min flow rate. The focused particle stream was tracked by a multilaser tracking system [8]. The aerodynamic diameter of each particle was determined from its terminal velocity [8, 9] and provided the necessary timing to fire either the 355- or 266-nm Nd:YAG desorption/ionization lasers.

Published online September 29, 2005

Address reprint requests to Carlito B. Lebrilla, Department of Chemistry, University of California-Davis, One Shields Avenue, Davis, CA 95616, USA. E-mail: cblebrilla@ucdavis.edu

1044-0305/05/$30.00
doi:10.1016/j.jasms.2005.06.013

Received March 7, 2005
Revised June 27, 2005
Accepted June 28, 2005

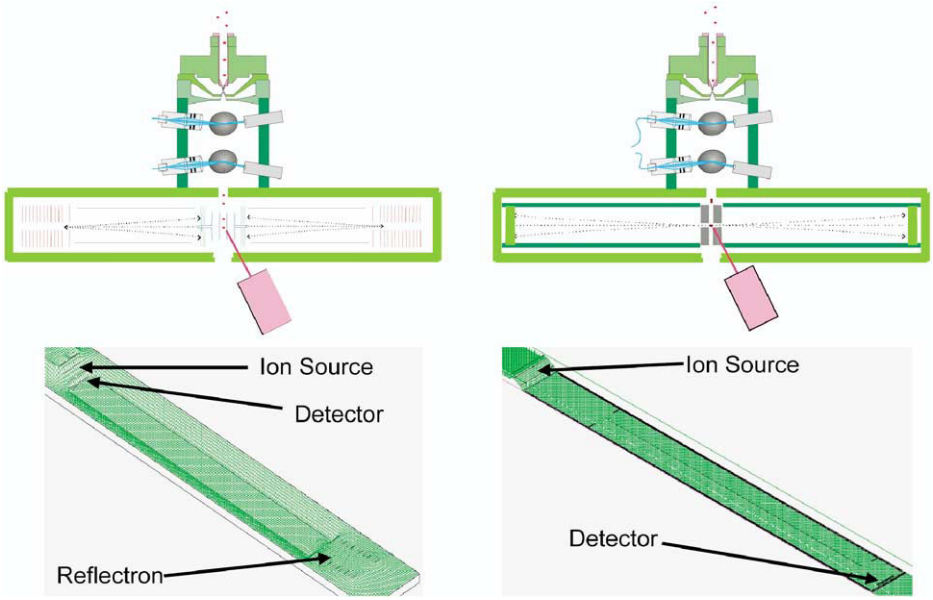

Figure 1. (**a**) Schematic and potential energy surface of the aerosol mass spectrometer in reflectron mode. (**b**) Schematic and potential energy surface of the aerosol mass spectrometer in linear mode.

Mass Spectrometry

A dual-polarity linear TOF instrument, shown in Figure 1, was fabricated with delayed extraction, pulsed ion guide, and postacceleration capabilities. The source dimensions, optimized via SIMION, were $S = 0.362$ in. and $D = 0.185$ in (Figure 2). The total length of each flight tube from the last extraction grid to microchannel plate (MCP) surface was 21.4 in. Extraction grids consisted of 1-in.-diameter fine nickel mesh (100 lines per in./80.1% transmission). To obtain a uniform field, the mesh was compressed and stretched between two stainless steel mounts. Kel-F was used as the insulating material between extraction grids. Each ion guide consisted of a 0.125-mm-diameter stainless steel wire mounted 10 cm away from extraction grids 1, 4, and 5 cm away from the end of each flight tube. The ion guide wires were supported by 0.0625-in. stainless steel crossbars at each end and pulled taught. The crossbars were moved 5 mm off axis to reduce potential ion collisions with the wire [10]. Photo-decoupled MCP detectors (Burle Electro-optics, Lancaster, PA) with a 25-mm detection surface were mounted to the end of each flight tube through Kel-F insulators and powered by Burle power supplies. Electrical isolation of the detectors from the flight tubes allowed for postacceleration capabilities.

The mass spectrometer is initialized with a TTL (Transistor Transistor Logic) pulse sent from the tracking algorithm that drives three DG535 pulse generators (Stanford Research Systems, Sunnyvale, CA; Figure 2). Pulse generators 2 and 3 provide timed TTL pulses to trigger laser firing and data digitization. Before ion extraction occurs a field free region is established in the first extraction stage by holding Grids 2 and 3 at −200 V. For the gramicidin S analysis, Grids 1 and 4 were set to −5 and +5 kV, respectively. After a time delay (τ) Grid 3 is pulsed from −200 V to +2 kV by a TTL pulse sent from pulse generator 1 to HV (high voltage) switch 2 and positive and negative ions are extracted into separate TOF analyzers. Inside the flight tubes, ions are initially repelled by the guide wire for some time D_1 after which the guide wires are switched to attracting potentials by HV switches 1 and 3. Typical delay times (τ) required for delayed extraction ranged from 100 to 600 ns, and delays for ion gating (D_1) ranged from 2 to 5 μs, depending on the m/z to be gated. Guide wire voltages used for repelling and attracting the ions ranged from ±100 to ±200 V relative to the flight tube.

Simion Modeling

The design of an aerosol TOF is subject to several unique complexities inherent to aerosol instruments. Although the parameters affecting resolution [11–14] and sensitivity performance [15] of conventional TOF analyzers is well documented, those pertaining specifically to aerosol mass spectrometry still have to be adequately addressed. This study presents a thorough analysis of the reflectron and linear BAMS instruments (with and without the guide wire) using SIMION 7.0. Ion transmission efficiencies, defined as the percentage of ions that impact the detector surface for a given m/z value, were determined to assess instrument sensitivity. Ion trajectories provided a visual representation of instrument performance and ion loss.

Reflectron Instrument Model

Voltages assigned to each electrode in the model were identical to those optimized empirically. Figure 1a

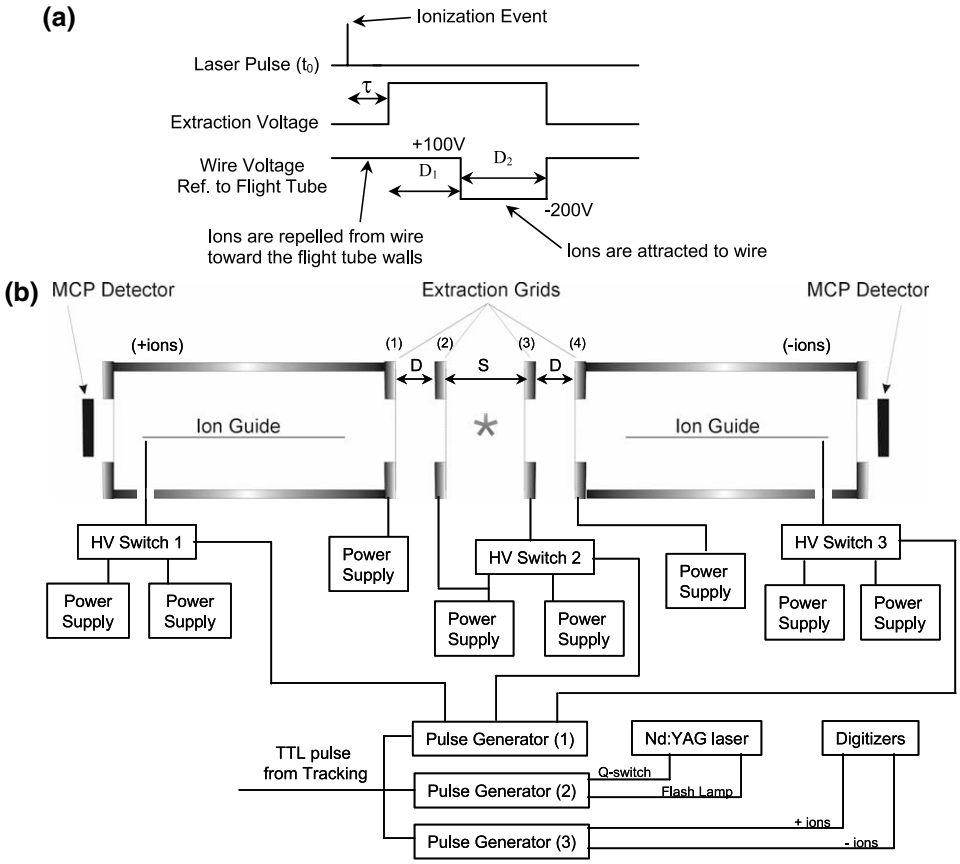

Figure 2. (**a**) Pulse diagram for an experiment involving both delayed extraction along with a pulsed guide wire. (**b**) Schematic of the dual-polarity linear TOF equipped with a dual-stage delayed extraction ions source and pulsed guide wires.

shows a schematic and the potential energy surface of the reflectron instrument. Generated ions are accelerated through a two-stage electrostatic-lens source, into the drift region (measuring 23.3 in.), and enter an on-axis ring electrode. Ions are then reflected back toward the detector located near the source.

Linear Instrument Modeling

The linear BAMS instrument was constructed in SIMION using the electrode dimensions cited in the experimental section. The potentials used for assessing ion transmission (using positive ions) were −5 kV on the flight tube, with −1.5 and 2.5 kV applied to the source plates. The ion guide was pulsed from −4.8 kV (repelling) to −5.2 kV (attracting) in both the modeling and the MALDI particle experimental studies in which the design was implemented. Delayed extraction was not modeled in the ion transmission studies. The potentials were set to those shown to produce high *m/z* signals from cytochrome C. For the SIMION analysis of gramicidin S with delayed extraction, extraction voltages of −200 and 1500 V were used. Again, these voltages were optimized empirically for gramicidin S. Delay extraction times were varied from 0 to 500 ns.

Initial Ion Conditions

The nature of the desorption process is particularly relevant in the modeling and design of a high mass aerosol TOF instrument. The initial desorption/ionization characteristics of the ions are linked to the overall TOF and therefore are inherently coupled to the instrument's resolution [14]. Instrument sensitivity relies on the transmission efficiency of ions from the desorption plume to the detector.

The nature of the ablated material from aerosol particles is dependent on their composition and morphology [16, 17]. It has been shown that laser ablation from a particle consisting of an absorbing core surrounded by a nonabsorbing exterior results in an ion plume approximating an exploding sphere [16]. This is referred to as the total ablation plume model. On the other hand, a strongly absorbing particle of homogeneous composition will result in desorption of material limited to within ~10 nm of the particle surface, [6, 17], which results in an ion plume directed back toward the ionizing laser. To understand instrument performance from both types of particles, both initial ion plume conditions were considered in this study. These ionization conditions are contrary to those of traditional TOF

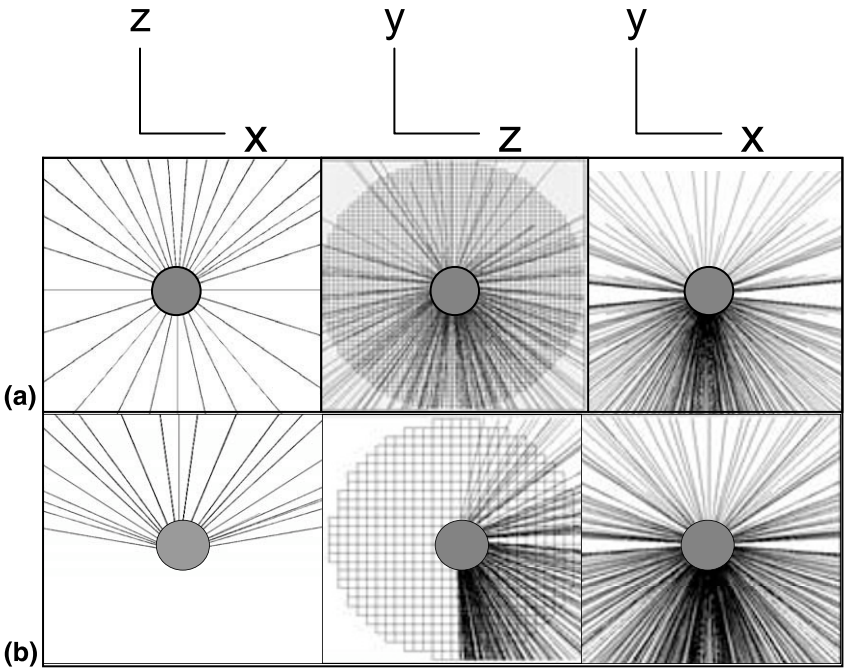

Figure 3. (**a**) Total ablation SIMION ion plume. (**b**) Partial ablation SIMION ion plume. Both plumes were modeled with Gaussian velocity distributions centered around 650 m/s coupled with a downward particle velocity vector of 350 m/s.

analyzers, in which the sample is ionized from a metal surface mounted orthogonal to the TOF axis. In these cases, the ion plume is directed along the TOF axis [18-20].

In BAMS, the velocity of a 1.0-micron aerosol particle at the time of desorption/ionization is roughly 350 m/s. The kinetic energy of the entering particle is conserved in the material ablated from the particle. Therefore, a downward particle velocity vector of 350 m/s was incorporated in all ion plumes. The resultant initial velocity and direction of the desorbed material is determined from the particle's initial kinetic energy and that imparted during the desorption/ionization event.

Using the initial ion velocities found experimentally, the mean initial ion velocity was modeled at 650 m/s [21, 22]. Wide velocity distributions about the mean have been observed in the laser desorption plume and were incorporated into the SIMION ion plume [23]. In the case of the spherical or total ablation ion plume, 1229 ions for each *m/z* were evenly dispersed over the entire solid angle of a sphere. The ions were modeled having a range of desorption velocities, centered at 650 m/s (449 ions), with slower ions at 450 m/s (136 ions) and 550 m/s (254 ions) and faster ions at 750 m/s (254 ions) and 850 m/s (136 ions; Figure 3a).

In the case of ablation from a homogeneously absorbing particle, partial ablation from the surface is expected [24]. This was modeled with the direction of the ion ablation assuming a broad cone of solid angle measuring 4.8 radians [2] (Figure 3b) to mimic the findings of Garrison et al. [16, 17, 24]. The ion plume was centered orthogonal to the TOF axis and directed back toward the ionization laser. The velocity distribution was centered at 650 m/s (256 ions), with additional ion velocities at 450 m/s (128 ions), 550 m/s (63 ions), 750 m/s (128 ions), and 850 m/s (63 ions).

Results

SIMION Modeling of Reflectron TOF

Through modeling, several shortcomings of the reflectron geometry used in the original BAMS instrument were made apparent. The trajectories of ions *m/z* 23, 100, 500, 1000, 1500, and 2000 were recorded. Velocity components perpendicular to the ion optical axis resulted in poor ion transport to the detector. Two factors contributed to the off-axis trajectories of the accelerated ions. The first was that of the particle velocity in the direction of the laser (*y*-direction) at the time of ionization. The second, and more significant, was the larger desorption velocities imparted on ions during ionization. These artifacts of the ionization plume were conserved in the trajectories of the accelerated ions. This results in many ions colliding with the flight tube before reaching the detector. The transport efficiency of larger ions (>500 *m/z*), because of their longer flight times, were more severely affected than smaller massed ions. Representative trajectories of *m/z* values 100 and 2000 from the partial ablation models are shown in Figure 4. Transmission efficiencies of ions from the partial ablation model within the reflectron system were *m/z* 23 (54%), *m/z* 100 (32%), *m/z* 500 (4.6%), *m/z* 1000 (1.6%), *m/z* 1500 (1.3%), and *m/z* 2000 (0.6%; Figure 5a). The transmission

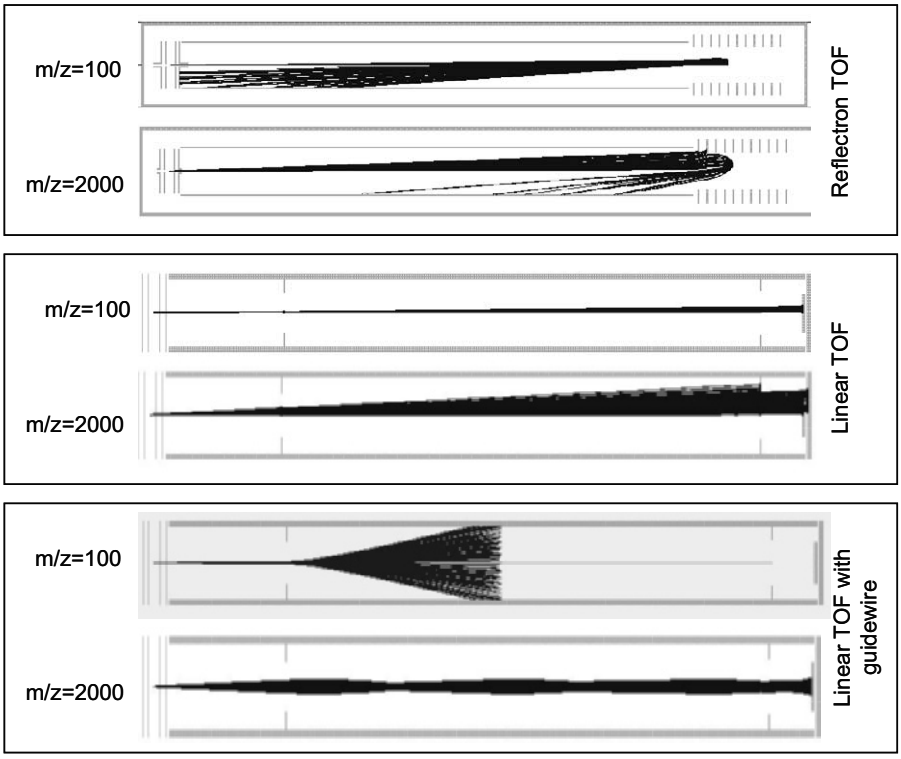

Figure 4. Ion trajectory plots for ions of *m/z* values 100 and 2000 with initial plume velocities centered around 650 m/s for reflectron, linear, and linear with guide wire models.

efficiencies of ions generated from the total ablation model were slightly better: *m/z* 23 (73%), *m/z* 100 (30%), *m/z* 500 (6.0%), *m/z* 1000 (3.5%), *m/z* 1500 (1.6%), and *m/z* 2000 (1.3%; Figure 5b).

SIMION Modeling of Linear TOF (With and Without Ion Guide)

A linear version of the instrument was also modeled in SIMION and is shown in Figure 1b. To provide a more uniform electric field within the ion source, 1-in.-diameter mesh extraction grids were modeled to replace the electrostatic ion lenses present in the reflectron design. A large detection surface, 25 mm in diameter, was chosen to compensate for the divergent ion trajectories encountered with the aerosol desorption/ionization event. An electrostatic ion guide was modeled by placing a single electrode down the flight tube. This electrode was pulsed via a user-defined program (see Figure 2a). Instrument performance with and without the ion guide was assessed using SIMION.

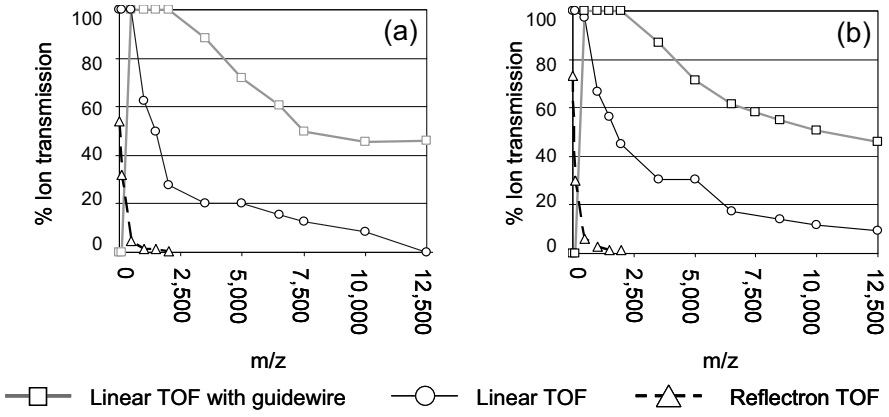

Figure 5. Ion transmission efficiencies versus *m/z* values from 0 to 12,500 for the reflectron, linear, and linear + guide wire models. (**a**) Full particle ablation with a Gaussian distribution of velocities centered around 650 m/s. (**b**) Partial particle ablation with a Gaussian distribution of velocities centered around 650 m/s.

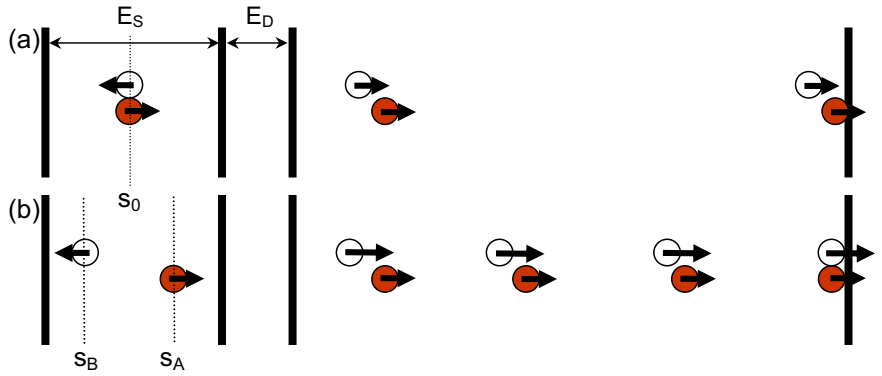

Figure 6. (**a**) Ions with the same initial position (s_0) but different velocities ($+v_0$ and $-v_0$) in a static extraction field arrive at the detector at different times. (**b**) The same ions allowed to evolve in a field-free environment and extracted at a delayed time t arrive at the detector together in time.

Improved ion transmission was observed in the linear instrument, as shown in Figure 4. Because of the shorter flight times in the linear instrument relative to the reflectron design, it is more tolerable of off-axis velocities. For ions up to *m/z* 500, the model predicted 100% transmission from the partial ablation plume. For larger masses, efficiency dropped to 63% for *m/z* 1000, 50% for *m/z* 1500, and 27% for *m/z* 2000 (Figure 5a). From the total ablation model, transmission efficiencies in the linear TOF again were slightly better: 100% (*m/z* 23), 100% (*m/z* 100), 97% (*m/z* 500), 67% (*m/z* 1000), 56% (*m/z* 1500), and 45% (*m/z* 2000; Figure 5b). The overall significance of the plume type played a minor role in instrument sensitivity, as evidenced by the calculated transmission efficiencies for both the linear and the reflectron TOF systems.

To fully compensate for the expanding plume, an electrostatic ion guide was implemented into the design to correct divergent ion trajectories. Electrostatic ion guides have proven successful at improving the signal-to-noise ratio (S/N) of plasma desorption TOF instruments in which ionization occurs from a static source [25, 26]. This technique has also been successfully applied to traditional MALDI-TOF systems [27]. The ion guide performs two functions: to collimate the trajectories of divergent ions, which improves ion transmission to the detector, and to gate low *m/z* ions that commonly saturate MCP detectors.

In MALDI, intense signals from low *m/z* matrix ions reach the detector first and deplete the charge on the MCP [28]. The charge must be replenished for optimal performance. The time required for a channel in the MCP array to recover is long (~20 ms) compared with the time for the analyte ions to reach the detector (~10 μs) [28]. The result is a diminished signal for larger *m/z* analyte ions and degraded instrument sensitivity.

Ion gating is performed by initially maintaining the ion guide wire at a repulsive potential relative to the flight tube. This accelerates the ions radially (outward) from the flight tube center. Smaller ions will be accelerated more than larger ions and will collide with the flight tube. Pulsing the ion guide to an attracting potential collimates the remaining high mass ions on a trajectory toward the detectors. This pulsed configuration allows for gating of low mass ions while simultaneously collimating high mass ions. The electrostatic ion guide was modeled in SIMION and the ion trajectory results are shown in Figure 4c. Ions of *m/z* 100 and under were repelled and impacted the flight tube walls. After the delay time D_1, the voltage was switched to an attracting potential. The higher mass ions were directed down the flight tube to the detector, yielding high transmission efficiencies. Using the partial ablation model, transmission efficiencies of 100% (*m/z* 500), 100% (*m/z* 2000), 72% (*m/z* 5000), and 46% (*m/z* 12,500) were achieved (Figure 5a). Similar values were recorded using the total ablation ion model (Figure 5b). Clearly, implementing the ion guide greatly improved overall ion transmission relative to the linear TOF without the ion guide.

Retaining Resolving Power (Delayed Extraction)

Although switching to a linear design with a guide wire increases instrument sensitivity, removing the reflectron sacrifices resolving power. If a linear instrument is to be effective, resolving power at higher masses must be conserved. To regain resolving power, delayed extraction was implemented in the design. Delayed extraction, or time-lag focusing, was originally developed by Wiley and Mclaren in 1955 [14]. More recently, this technique has been applied to MALDI from a surface to correct for the inherent initial velocity distribution resulting from the desorption/ionization event [11-13]. In the case of single particle ionization, as opposed to ionization from a plate, initial ion velocities are not obstructed by the sample probe surface. The generated ions can be directed toward and away from the detector. To illustrate this, Figure 6a depicts two ions (A and B) formed at the same position (s_0) but with different initial velocities $+v_0$ and $-v_0$ in a static accelerating field. Ion A, which is moving toward the detector, is accelerated and enters the field-free region first. Ion B, which is moving away from the detector must first

decelerate and then be accelerated in the direction of the detector. Consequently, ion B lags behind ion A, leading to different arrival times for the same m/z value (Figure 6a).

If these same two ions are allowed to evolve in a field-free environment, they will move to new positions s_A and s_B, given by eqs 1 and 2, respectively.

$$S_A = S_0 + v_0\tau \tag{3a}$$

$$S_B = S_0 - v_0\tau \tag{3b}$$

After a time delay τ, the electric field is applied and the two ions are accelerated to final kinetic energies according to eqs 3 and 4, where m is mass, q is charge in Coulombs, E_S is the electric field in the first extraction stage, E_D is the electric field in the second extraction region, and d is the distance of the second extraction region.

$$KE_A = \frac{1}{2}mv_0^2 + qE_{s_{s_A}} + qE_D d \tag{4a}$$

$$KE_B = \frac{1}{2}mv_0^2 + qE_{s_{s_B}} + qE_D d \tag{4b}$$

Because the amount of kinetic energy imparted on each ion depends on their position in the source at the time of extraction ($s_A < s_B$), the backward moving ion B will enter the field-free region with a higher kinetic energy than ion A. Using the correct delay time (τ), ion B will be accelerated sufficiently to catch up to ion A and both ions will impact the detector at the same time (Figure 6b).

Experimental Effects of Delayed Extraction

An assessment of the delayed extraction via single particle MALDI experiments and SIMION modeling was performed. Single particle MALDI experiments involved aerosols composed of a mixture of DHB and gramicidin S (100:1). In SIMION, modeled ions of m/z 1141 corresponding to [gramicidin:Na]$^+$ were modeled using both the partial ablation and total ablation ion plume models. Modeling of both ion plumes necessary to assess the ability of delayed extraction to energy focus ions of both plumes must be addressed. Extraction delays from 0 to 500 ns were studied. Average resolution for the experimental data were calculated as $m/\Delta m$ at full width at half maximum (FWHM) for the [M + Na]$^+$ gramicidin S. Only peaks with intensity greater than 50 were considered to ensure representative FWHM calculations. From the SIMION modeling data, resolution was estimated by calculating the standard deviation σ of the ion flight times. By assuming a Gaussian distribution of flight times, the Δt FWHM of the SIMION data were approximated by $2.3 \times \sigma$. From the approximated Δt, the resolution can then be determined by $t/2\Delta t$, which is equivalent to $m/30>m$ [14]. Calculations in this manner provided a means of comparing ion focusing between the modeled data and the experimental data on the same scale.

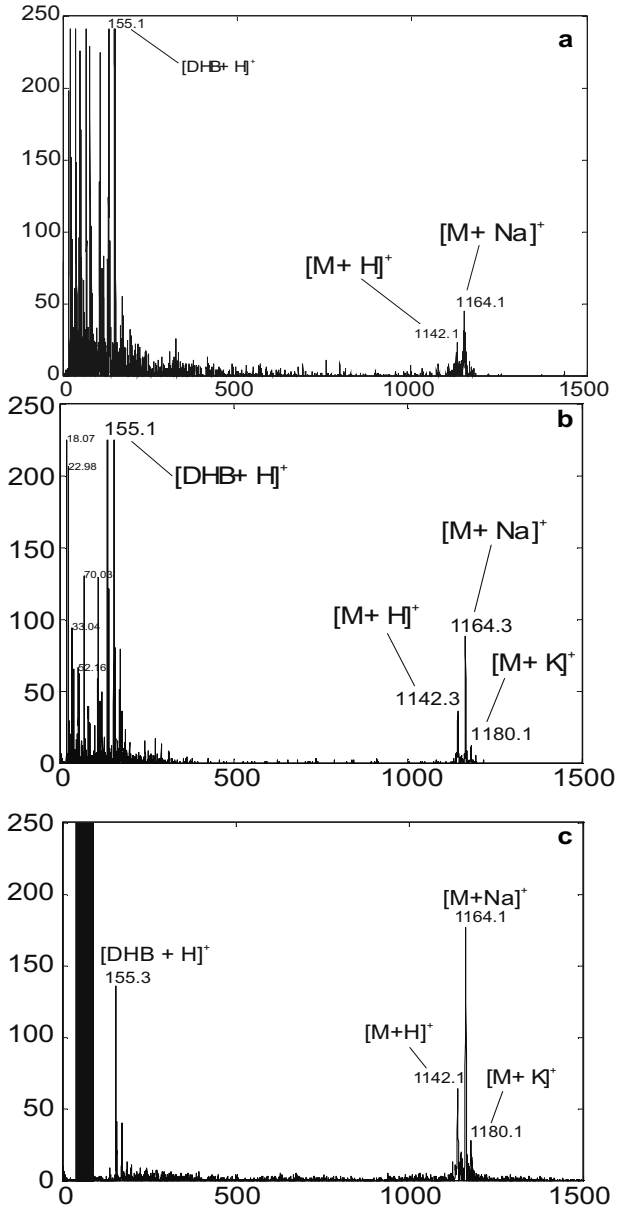

Figure 7. (**a**) Mass spectra of DHB:gramicidin S single particles generated from a solution containing 100:1 matrix to analyte ratio. (**a**) A 0.7-μm single particle acquired with no delayed extraction or guide wire; (**b**) 0.8-μm single particle acquired with a time lag τ = 350 ns but no guide wire; (**c**) 0.8-μm single particle acquired with a time lag τ = 350 ns and guide wire delay D_1 = 4 μs. The black rectangle is a result of pulsing of voltages for the guide wire.

At zero delay time the average experimental resolution was 177 for the [M + Na]$^+$ molecular ion at m/z 1164. A representative single particle spectrum is shown in Figure 7a. In this spectrum only two quasi-molecular ions were observed for gramicidin S, namely, [M + H]$^+$ and [M + Na]$^+$ at m/z values 1142.1 and 1164.1, respectively. Increasing the delay time (τ) pro-

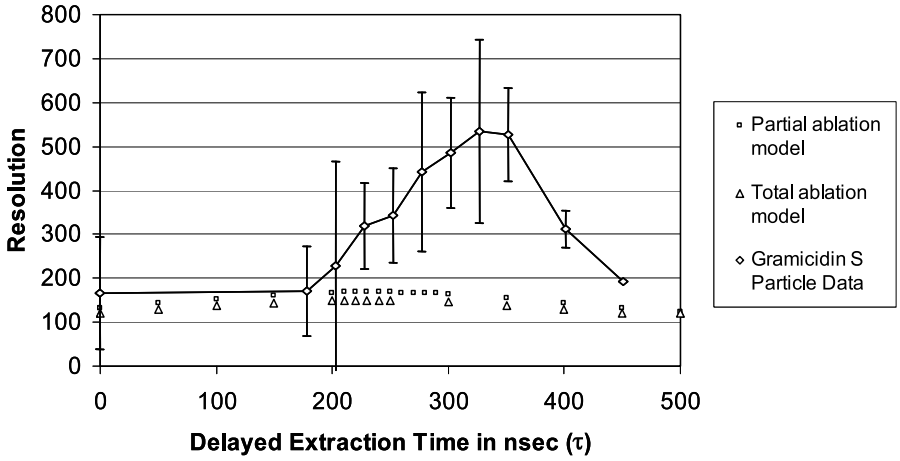

Figure 8. Plot of resolution as a function of delayed extraction time (τ) for both plume models and experimental gramicidin S data.

vided a threefold improvement in average resolution to a maximum of 523 at τ = 323 ns. Improving the resolution also increases the S/N ratio of the analyte peaks and improves the likelihood of detection of biomarker peaks. For instance, at improved resolution, three quasi-molecular ions [M + H], $[M + Na]^+$, and $[M + K]^+$ were observed at *m/z* values 1142.3, 1164.3, and 1180.1, respectively. A representative single particle spectrum is shown in Figure 8b. The results for peak resolution at delay times ranging from 0 to 500 ns are plotted in Figure 8. Plotted alongside the experimental data is the resolution estimated from SIMION. The optimal average resolution 532 is higher than that estimated from the SIMION models for the partial and total ablation plume 170 and 149, respectively. It was also found that the optimal delayed extraction time τ differed between the SIMION data and the experimental data. The experimentally optimized delay time was found to be 323 ns. The resulting optimal delay times from SIMION were 250 ns for both the total and the partial ablation plume models. It is evident that the full benefits of delayed extraction are not realized in the SIMION model. The discrepancies between the model and experimental data could originate from model plume velocities and dynamics that do not match the experimental reality. Experimentally, the optimal delay times were found to be larger than those predicted by the SIMION models. This could indicate that ion initial velocities are actually faster than those portrayed in the SIMION model. Also, the overall predicted resolution is significantly lower than in the experimental data. The SIMION model does not account for in-plume ion collisions and delayed ion formation, which could explain the inaccuracies of the model. Nevertheless, these results show a successful application of delayed extraction to improve resolution of high mass ions generated from micrometer-size particles.

The optimal delay time for extraction in TOF is *m/z* dependent. This effect is expected to be more pronounced in BAMS because of the plume dynamics from laser ablated aerosols. The delay time dependence of gramicidin S (*m/z* 1164.3) resolution depicted in Figure 7 indicates that within 50 ns of the optimal delay (323 ns), resolution degrades by roughly 20%. The optimal delay time for cytochrome C (*m/z* ~12,000) was found to be 350 ns and is only slightly longer than that for gramicidin S. This illustrates that although optimal delay times for a wide range of analytes may not be possible, satisfactory resolution for all analytes may be achieved at a single delay time. Additional studies characterizing optimal delay extraction time dependence on *m/z* for aerosol particle ionization is ongoing in our laboratory and will be included in a forthcoming publication.

Experimental Results with the Guide Wire

The affect of the guide wire at higher masses was evaluated experimentally with particles consisting of DHB and gramicidin S. This system has been used previously to evaluate the performance of a guide wire for ionization occurring from a sample plate [10]. The matrix peaks provide abundant ions at the low mass range whereas gramicidin S provides higher mass molecular ions of $[M + H]^+$, $[M + Na]^+$, and $[M + K]^+$ at *m/z* values 1141, 1165, and 1180, respectively. Figure 7b is a single particle spectrum acquired with a $[M + Na]^+$ peak height representative of the average. This spectrum was acquired with a delayed extraction time of 350 ns but without the guide wire. Although the molecular ions are nicely resolved, many low mass matrix peaks are still detected and may lead to detector saturation. Figure 7c is a single particle spectrum of the same sample but with the ion guide operating with a D_1 time of 4 μs. In this configuration most *m/z* values below 150 have been gated out, whereas *m/z* values above are collimated down the flight tube to the detector. In this model system, high mass sensitivity was increased by using the guide wire, which supports the SIMION modeling presented previously. Experimen-

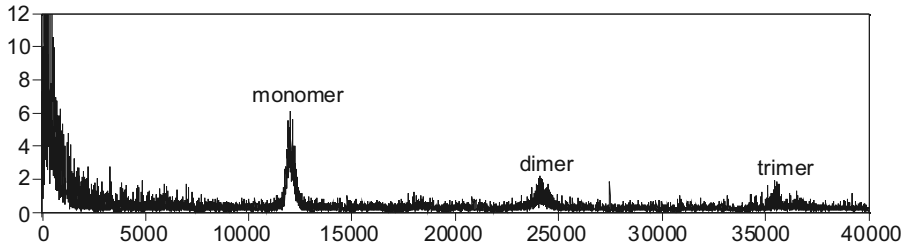

Figure 9. Average of 27 cytochrome C:sinapinic acid single particle spectra. Monomer, dimer, and trimer peaks were observed at 12, 24, and 36 kDa, respectively. Spectra were acquired with a time lag of 350 ns and guide wire delay D_1 of 3 μs.

tally, an approximately twofold increase in signal intensity was observed by implementing the ion guide (Figure 8c). This result is in agreement with SIMION, which predicted an increase in ion transmission from 62 to 100% for *m/z* 1000 when using the ion guide (Figure 5a, b).

The mass range was pushed further by analyzing particles containing sinapinic acid and cytochrome C. An average spectrum of 27 cytochrome C:sinapinic acid particles is shown in Figure 9. The molecular ion was observed at 12 kDa along with signals corresponding to a dimer and trimer at 24 and 36 kDa, respectively. These high mass spectra were obtained with a delayed extraction time (τ) of 350 ns and guide wire delay D_1 of 3.0 μs. Postacceleration voltage of 1 kV also was used to increase the kinetic energy of the ions on impact with the MCP detector. Detection of the high mass signals confirms the mass range of the BAMS instrument has been improved.

Conclusion

The BAMS reflectron TOF and linear TOF with electrostatic ion guide have been compared experimentally and with SIMION modeling. The modeling revealed that divergent ion trajectories from desorption/ionization resulted in poor ion transmission and reduced sensitivity. The effect is amplified at higher *m/z* values because of longer ion flight times. The reflectron TOF analyzer transmitted less than 2% of ions with *m/z* 2000. Ion transmission was improved through a linear geometry TOF, with 28 and 45% ion transmission for the partial and total ablation model, respectively. Implementing the ion guide wire improved the transmission even further, with 100% transmission for both SIMION models. Ion transmission efficiencies for *m/z* 10,000 were 45 and 50% for the partial and total ablation models, respectively. The ion guide proved to be effective in gating low *m/z* ions from the detector while collimating higher *m/z* ions, resulting in improved S/N. Delayed extraction resulted in an experimental resolution of 531 ($\Delta m/m$, at FWHM) for *m/z* 1164 for sodiated gramicidin S. This performance was comparable with that obtained in the reflectron TOF. This represents an approximately threefold improvement, from resolution 177, compared with when delayed extraction was not used. Overall, the instrument sensitivity was greatly improved, with little or no loss from overall resolution.

Acknowledgments

This work was performed under the auspices of the U.S. Department of Energy by University of California Lawrence Livermore National Laboratory under Contract W-7405-ENG-48. This project was funded by the Technical Support Working Group of the Department of Defense. Scott Russell and Gregg Czerwieniec acknowledge the LLNL Student Employee Graduate Research Fellowship (SEGRF) for support. Funding from the National Science Foundation (CBL) is also appreciated.

References

1. Czerwieniec, G. A.; Russell, S. C.; Tobias, H. J.; Pitesky, M. E.; Fergenson, D. P.; Steele, P.; Srivastava, A.; Horn, J. M.; Frank, M.; Gard, E. E.; Lebrilla, C. B. Stable Isotope Labeling of Entire *Bacillus atrophaeus* Spores and Vegetative Cells Using Bioaerosol Mass Spectrometry. *Anal. Chem.* **2005,** *77,* 1081–1087.
2. Fergenson, D. P.; Pitesky, M. E.; Tobias, H. J.; Steele, P. T.; Czerwieniec, G. A.; Russell, S. C.; Lebrilla, C. B.; Horn, J. M.; Coffee, K. R.; Srivastava, A.; Pillai, S. P.; Shih, M. T. P.; Hall, H. L.; Ramponi, A. J.; Chang, J. T.; Langlois, R. G.; Estacio, P. L.; Hadley, R. T.; Frank, M.; Gard, E. E. Reagentless Detection and Classification of Individual Bioaerosol Particles in Seconds. *Anal. Chem.* **2004,** *76,* 373–378.
3. Beeson, M. D.; Murray, K. K.; Russell, D. H. Aerosol Matrix-Assisted Laser-Desorption Ionization—Effects of Analyte Concentration and Matrix-to-Analyte Ratio. *Anal. Chem.* **1995,** *67,* 1981–1986.
4. Fei, X.; Wei, G.; Murray, K. K. Aerosol MALDI with a Reflectron Time-of-Flight Mass Spectrometer. *Anal. Chem.* **1996,** *68,* 1143–1147.
5. He, L.; Murray, K. K. 337 nm Matrix-Assisted Laser Desorption/Ionization of Single Aerosol Particles. *J. Mass. Spectrom.* **1999,** *34,* 909–914.
6. Mansoori, B. A.; Johnston, M. V.; Wexler, A. S. Matrix-Assisted Laser Desorption/Ionization of Size- and Composition Selected Aerosol Particles. *Anal. Chem.* **1996,** *68,* 3595–3601.
7. Stowers, M. A.; van Wuijckhuijse, A. L.; Marijnissen, J. C. M.; Scarlett, B.; van Baar, B. L. M.; Kientz, C. E. Application of Matrix-Assisted Laser Desorption/Ionization to On-Line Aerosol Time-of-Flight Mass Spectrometry. *Rapid Commun. Mass Spectrom.* **2000,** *14,* 829–833.
8. Coffee, K. R. Manuscript in preparation. **2005**.
9. Gard, E. E.; Mayer, J. E.; Morrical, B. D.; Dienes, T.; Fergenson, D. P.; Prather, K. A. Real-Time Analysis of Individual Atmospheric Aerosol Particles—Design and Performance of a Portable ATOFMS. *Anal. Chem.* **1997,** *69,* 4083–4091.
10. Hanson, C. D.; Just, C. L. Selective Background Suppression in MALDI-TOF Mass-Spectrometry. *Anal. Chem.* **1994,** *66,* 3676–3680.

11. Whittal, R. M.; Li, L. High-Resolution Matrix-Assisted Laser Desorption Ionization in a Linear Time-of-Flight Mass-Spectrometer. *Anal. Chem.* **1995,** *67,* 1950–1954.
12. Vestal, M. L.; Juhasz, P.; Martin, S. A. Delayed Extraction Matrix-Assisted Laser-Desorption Time-of-Flight Mass-Spectrometry. *Rapid Commun. Mass Spectrom.* **1995,** *9,* 1044–1050.
13. Brown, R. S.; Lennon, J. J. Mass Resolution Improvement by Incorporation of Pulsed Ion Extraction in a Matrix-Assisted Laser-Desorption Ionization Linear Time-of-Flight Mass-Spectrometer. *Anal. Chem.* **1995,** *67,* 1998–2003.
14. Wiley, W. C.; McLaren, I. H. Time-of-Flight Mass Spectrometer with Improved Resolution (Reprinted from *Review of Scientific Instruments*, **26**, 1995, p. 1150). *J. Mass Spectrom.* **1997,** *32,* 4–11.
15. Keller, B. O.; Li, L. Detection of 25,000 Molecules of Substance P by MALDI-TOF Mass Spectrometry and Investigations into the Fundamental Limits of Detection in MALDI. *J. Am. Soc. Mass Spectrom.* **2001,** *12,* 1055–1063.
16. Schoolcraft, T. A.; Constable, G. S.; Jackson, B.; Zhigilei, L. V.; Garrison, B. J. Molecular Dynamics Simulations of Laser Disintegration of Amorphous Aerosol Particles with Spatially Nonuniform Absorption. *Nucl. Instrum. Methods Phys. Res. B* **2001,** *180,* 245–250.
17. Schoolcraft, T. A.; Constable, G. S.; Zhigilei, L. V.; Garrison, B. J. Molecular Dynamics Simulation of the Laser Disintegration of Aerosol Particles. *Anal. Chem.* **2000,** *72,* 5143–5150.
18. Zhang, W. Z.; Chait, B. T. Radial Velocity Distributions of Molecular Ions Produced by Matrix-Assisted Laser Desorption/Ionization. *Int. J. Mass Spectrom.* **1997,** *160,* 259–267.
19. Spengler, B.; Bokelmann, V. Angular and Time-Resolved Intensity Distributions of Laser-Desorbed Matrix Ions. *Nucl. Instrum. Methods B* **1993,** *82,* 379–385.
20. Puretzky, A. A.; Geohegan, D. B.; Hurst, G. B.; Buchanan, M. V.; Luk'yanchuk, B. S. Imaging of Vapor Plumes Produced by Matrix Assisted Laser Desorption: A Plume Sharpening Effect. *Phys. Rev. Lett.* **1999,** *83,* 444–447.
21. Berkenkamp, S.; Menzel, C.; Hillenkamp, F.; Dreisewerd, K. Measurements of Mean Initial Velocities of Analyte and Matrix Ions in Infrared Matrix-Assisted Laser Desorption Ionization Mass Spectrometry. *J. Am. Soc. Mass Spectrom.* **2002,** *13,* 209–220.
22. Spengler, B.; Kirsch, D. On the Formation of Initial Ion Velocities in Matrix-Assisted Laser Desorption Ionization: Virtual Desorption Time as an Additional Parameter Describing Ion Ejection Dynamics. *Int. J. Mass Spectrom.* **2003,** *226,* 71–83.
23. Karas, M.; Bahr, U.; Fournier, I.; Gluckmann, M.; Pfenninger, A. The Initial-Ion Velocity as a Marker for Different Desorption-Ionization Mechanisms in MALDI. *Int. J. Mass Spectrom.* **2003,** *226,* 239–248.
24. Zhigilei, L. V.; Garrison, B. J. Computer Simulation Study of Damage and Ablation of Submicron Particles from Short-Pulse Laser Irradiation. *Appl. Surf. Sci.* **1998,** *129,* 142–150.
25. Wolf, B.; Macfarlane, R. D. A Pulsed Ion Deflection System for Background Reduction in Cf-252-Plasma Desorption Mass-Spectrometry. *J. Am. Soc. Mass Spectrom.* **1992,** *3,* 706–715.
26. Geno, P. W.; Macfarlane, R. D. Cf-252 Plasma Desorption Mass-Spectrometry at Low Acceleration Voltages Using the Electrostatic Particle Guide. *Int. J. Mass Spectrom.* **1986,** *74,* 43–57.
27. Brown, R. S.; Gilfrich, N. L. Optimizing Signal and Mass Resolution for Matrix-Assisted Laser Desorption Utilizing a Linear Time-of-Flight Mass-Spectrometer. *Rapid Commun. Mass Spectrom.* **1992,** *6,* 697–701.
28. Wiza, J. L. Microchannel Plate Detectors. *Nucl. Instrum. Methods* **1979**, *162*, 587–601.